Magnetic anisotropy in clinopyroxene and orthopyroxene single crystals

Andrea R. Biedermann[1], Thomas Pettke[2], Christian Bender Koch[3] and Ann M. Hirt[1,*]

[1] Institute of Geophysics, ETH Zurich, Sonneggstrasse 5, 8092 Zurich, Switzerland

[2] Institute of Geological Sciences, University of Bern, Baltzerstrasse 1-3, 3012 Bern, Switzerland

[3] Department of Chemistry, University of Copenhagen, Universitetsparken 5, 2100 Copenhagen Ø, Denmark

The final version of this article is available from the JGR website, doi: 10.1002/2014JB011678

http://onlinelibrary.wiley.com/doi/10.1002/2014JB011678/abstract

Keywords

AMS (anisotropy of magnetic susceptibility); magnetic properties; single crystal

clinopyroxene; augite, diopside, spodumene, aegirine

orthopyroxene; enstatite

Abstract

Pyroxenes constitute an important component in mafic igneous and metamorphic rocks. They often possess a prismatic habit and their long axis, the crystallographic *c*-axis, helps define a lineation in a textured rock. Anisotropy of magnetic susceptibility (AMS) serves as a fabric indicator in igneous and metamorphic rocks. If a rock's AMS is carried by pyroxenes, it can be related to their crystallographic preferred orientation and degree of alignment. This requires knowing the intrinsic AMS of pyroxene single crystals. This study provides a comprehensive low-field and high-field AMS investigation of chemically diverse ortho- and clinopyroxene crystals in relation to crystal structure, chemical composition, oxidation state of Fe, and the possible presence of ferromagnetic inclusions. The paramagnetic anisotropy, extracted from high-field data, shows clear relationships to crystallographic directions and Fe concentration both in clino- and orthopyroxenes. In the diopside-augite series, the intermediate susceptibility is parallel to *b*, and the maximum is at 45° to the *c*-axis. In aegirine, the intermediate axis remains parallel to *b*, while the maximum susceptibility is parallel to *c*. The AMS of spodumene depends on Fe concentration. In enstatite, the maximum susceptibility aligns with *c* and the minimum with *b*, and in the case of hypersthene, the maximum susceptibility is normal to the exsolution lamellae. Magnetite inclusions within augite possess a ferromagnetic anisotropy with consistent orientation of the principal susceptibilities, which dominates the low-field anisotropy. These results provide better understanding of magnetic anisotropy in pyroxenes and form a solid basis for interpretation of magnetic fabrics in pyroxene-bearing rocks.

1 Introduction

Pyroxenes are common minerals in mafic and ultramafic igneous and metamorphic rocks. Orthopyroxene in particular is an important constituent of the Earth's upper mantle [*Deer et al.*, 1978]. Pyroxenes are single-chain silicates in which $(Si_2O_6^{4-})_n$ chains are linked by cations (Figure 1). The cations can occupy two non-equivalent sites, M1 and M2. In clinopyroxenes, the M2 site is strongly distorted with an irregular six- (spodumene) or eight-fold (augite, diopside, aegirine) coordination, and generally occupied by Ca, Na, K or Li. The M1 site is coordinated by a nearly regular octahedron and generally occupied by the smaller cations Mg, Fe^{2+}, Fe^{3+}, Mn, Al, Ti. Fe^{2+} is normally located in the M1 site, but if not enough Ca (or other large cations) is present to fully occupy M2, Fe^{2+} prefers M2 sites. Clinopyroxene is monoclinic with space group *C*2/*c*. Orthopyroxenes contain no significant amounts of Ca and due to the overall smaller radius of the cations in the M1 and M2 sites, their crystal structure is orthorhombic (space group *Pbca*). Similar to clinopyroxenes, orthopyroxenes possess M1 and M2 sites, where the M1 site is coordinated in an almost regular octahedron, and the M2 sites have a distorted six-fold coordination. Fe^{2+} prefers the M2 sites in orthopyroxenes [*Deer et al.*, 1978]. The structure of both pyroxene groups consists of long covalently bonded chains in the *c*-direction, which are linked by weaker ionic bonds in directions perpendicular to the chains; consequently clinopyroxenes and orthopyroxenes have well-defined cleavage on {110} and {210}, respectively [*Deer et al.*, 1978]. Therefore, pyroxenes often display prismatic habits and their *c*-axis aligns with the rock lineation, thus indicating flow directions or deformation in igneous and metamorphic rocks, respectively.

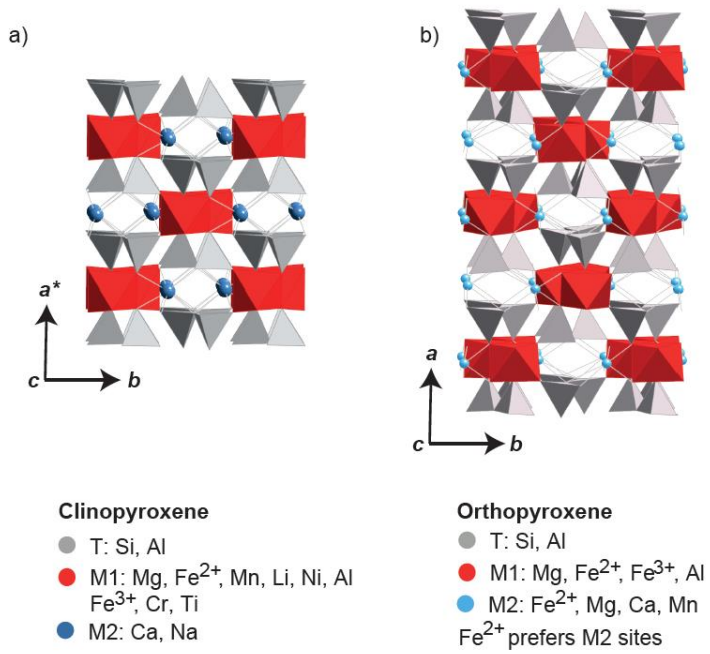

Figure 1: Crystal structure and typical site occupancies for clino- (a) and orthopyroxene (b). Figure generated with CrystalMaker.

Anisotropy of magnetic susceptibility (AMS) is often used as a proxy for rock texture [e.g. *Borradaile and Henry*, 1997; *Hrouda*, 1982, and references therein]. Magnetic susceptibility is a second-order tensor property, represented by a symmetric 3x3 matrix whose eigenvalues correspond to the principal susceptibilities $k_1 \geq k_2 \geq k_3$, and the respective eigenvectors reflect their directions. Magnetic anisotropy can be carried by ferromagnetic grains or by Fe-bearing silicates, e.g. pyroxene, with crystallographic preferred orientation. For example, the AMS of an aegirine-augite syenite from the Triunfo pluton in Brazil is controlled by aegirine-augite [*Archanjo and Bouchez*, 1997]. The authors found an oblate magnetic fabric and suggested that this may be caused by (1) an oblate single crystal AMS of the clinopyroxene, or (2) the compaction of the magma chamber after emplacement. A conclusive interpretation of the magnetic fabric was not possible, because the single crystal properties of clinopyroxenes are not well established. This study illustrates that a good

quantitative understanding of single-crystal magnetic properties is essential before using the magnetic fabric as a strain indicator.

At present, there are only a few studies on the intrinsic magnetic anisotropy of clinopyroxene and orthopyroxene crystals. Some of these indicate that the maximum susceptibility in pyroxene is not always parallel to the crystallographic *c*-axis. In the early 20th century, *Finke* [1909] measured one augite crystal and found that k_1 is at a -7° angle to the *c*-axis. Later, *Parry* [1971; cited in *Wagner et al.*, 1981] measured 19 augite crystals using high-field torque magnetometry and concluded that the intermediate susceptibility k_2 is always parallel to *b* and k_1 and k_3 lie in-between the *c*- and ±*a*-axes. *Lagroix and Borradaile* [2000] measured four clinopyroxenes, with a special focus on the ferromagnetic inclusions within the pyroxenes, and found that in three crystals the intermediate susceptibility is parallel to *b*, whereas no symmetry was found for k_1 or k_3. Two studies exist on orthopyroxenes; *Wiedenmann et al.* [1986] studied synthetic and natural Fe-rich orthopyroxene and found that k_1 is parallel to *b* and antiferromagnetic ordering sets in at sufficiently low temperatures. *Lagroix and Borradaile* [2000] measured five orthopyroxene samples and found that the maximum susceptibility is parallel to *c*. They did not find any relationship between k_2 and k_3 to either *a* or *b* and attributed this to ferromagnetic inclusions or misorientation.

These few investigations show no consistent relationship between the principal susceptibility axes and the crystallographic axes. Studies on other mineral groups have shown the influence of chemical composition on the degree of AMS and orientation of principal axes [*Almqvist et al.*, 2010; *Biedermann et al.*, 2014b; *Schmidt et al.*, 2007a]. The exact chemical composition of the crystals was only given in one study on orthopyroxene [*Wiedenmann et al.*, 1986]; therefore, little information is available on the effects of chemical composition, or

site distribution and oxidation state of Fe, which may vary considerably, on the magnetic properties.

In this study, a systematic investigation of magnetic anisotropy in clinopyroxene and orthopyroxene of various compositions is conducted. Bulk chemistry, oxidation states of Fe and site distributions are determined in order to gain a complete understanding of factors that influence the degree of paramagnetic anisotropy and the orientation of the principal axes with respect to the crystallographic axes.

2 Material and methods

2.1 Samples and sample preparation

Samples were collected to cover a wide range of chemical compositions and include crystals from the mineral groups diopside, augite, aegirine, spodumene and enstatite. Good-quality single crystals were obtained from different sources; (1) the Natural History Museum Basel (labeled NMB), (2) the ETH Mineral Collection, (3) mineral suppliers, and (4) field work in Tenerife and on Isola Vulcano. In addition, two hypersthene samples, consisting of lamellar intergrowth of clino- and orthopyroxene, were measured. An overview of samples and their localities is given in Table 1.

If needed, samples were first separated from the host rock. They were cleaned in ethanol in an ultrasonic cleaner and weighed. Crystal orientation was determined based on the crystal habit and Laue X-ray diffraction, which was performed at the Laboratory of Crystallography, ETH Zurich. Laue images were processed with the OrientExpress 3.4 crystal orientation software [*Laugier and Filhol*, 1983]. Based on Laue images obtained from different crystal faces, it was possible to identify twinning on {100} in some of the augite crystals and one aegirine crystal. Three of the aegirine samples showed a superposition of two

Laue patterns corresponding to two individual crystals with slightly different orientation. Because both features are common in clinopyroxene, these samples were also included in the study (cf. Table 1). The oriented samples were glued into cylindrical plastic holders for the magnetic measurements. Surfaces were polished prior to chemical analysis if required.

2.2 Chemistry

2.2.1 Bulk chemistry

Bulk chemical composition was determined using laser ablation inductively coupled plasma mass spectroscopy (LA-ICP-MS) at the Institute of Geological Sciences, University of Bern. LA-ICP-MS was preferred over electron probe microanalysis because LA-ICP-MS analyzes a several orders of magnitude larger sample volume per spot including possible inclusion materials (minerals or melt inclusions), and because entire crystals or large pieces thereof can be analyzed without the need for perfectly polished sections. Four to six spots were measured on crystal surfaces, polished crystal surfaces or/and cleavage planes for each sample. Measurements were performed with a beam diameter of 90 or 120 µm, after the surface had been cleaned with a larger beam. SRM610 and SRM612 from NIST were used for external standardization, with values reported in *Spandler et al.* [2011]. The measurement procedure and settings are described in *Pettke et al.* [2012]. The data was processed using SILLS [*Guillong et al.*, 2008], normalized to 100 wt.% total major oxides and averaged for further investigation. Note that additional information is needed in order to determine the oxidation state of Fe. Therefore, the total Fe concentration was determined assuming that all Fe is present as Fe^{2+} in diopside, augite, spodumene and the orthopyroxenes. For aegirine, it was assumed that all Fe is Fe^{3+}, according to the ideal chemical composition.

2.2.2 Mössbauer spectra

In order to determine the relative proportion of Fe^{2+} and Fe^{3+} in the crystals and investigate details in the coordination sites, Mössbauer spectra were measured of selected clinopyroxene samples. Absorbers were prepared by mixing powdered mineral samples and BN and transferring the mix into Perspex^{R} sample holders. Spectra were obtained at room temperature using a conventional constant acceleration spectrometer with the absorber perpendicular to the gamma ray direction. The spectrometer was calibrated using the spectrum of a thin foil of natural iron at room temperature and isomer shifts are given relative to the center of this absorber. The spectra were fitted using a combination of doublet components having Lorentzian line shape, and it was assumed that relative spectral areas are identical to relative abundances of the components.

2.2.3 Recalculation of mineral formulae

Mineral formulae were recalculated based on the assumption that four cations (including Si) are present per formula unit. The cations were then assigned to the tetrahedral sites within the chains, where Al can substitute for Si, and the M1 and M2 sites. Where Mössbauer data was available, the Fe^{3+} concentration was determined based on these. In order to test the analyses, the total positive charge, which should amount to 12, was calculated.

2.3 Magnetic measurements

2.3.1 Characterization of ferromagnetic inclusions

Many minerals, even single crystals, contain inclusions of other phases. For magnetic studies, ferromagnetic inclusions such as magnetite are of major interest, because they possess a large susceptibility. Hence, even small fractions of such inclusions strongly influence the bulk magnetic properties of the sample. Acquisition of isothermal remanent magnetization (IRM) was measured in order to verify the presence of ferromagnetic inclusions. The

magnitude of the saturation IRM provides an estimate of the concentration of ferromagnetic material in the sample. The crystals were magnetized first along the -*c* direction in a 2 T field using an ASC Scientific IM-10-30 Pulse Magnetizer. Subsequently the crystal was remagnetized along the +*c* direction in increasing fields between 20 mT and 2 T. The magnetization was measured on a 2G Enterprises, three-axis, cryogenic magnetometer (Model 755) after each step.

2.3.2 Magnetic susceptibility and anisotropy of magnetic susceptibility

Low-field susceptibility was measured on an AGICO MFK1-FA susceptibility bridge, in fields of 200 A/m or 500 A/m and a frequency of 976 Hz. Magnetic susceptibility was measured in 15 directions. Directional susceptibility measurements were repeated 10 times for each position and averaged, in order to receive the best possible signal quality [*Biedermann et al.*, 2013]. The full magnetic susceptibility tensor was computed from these directional measurements. Mean susceptibility (k_{mean}) is calculated as the arithmetic mean of the three eigenvalues of this tensor. The degree of the anisotropy will be described by $k' = \sqrt{[(k_1 - k_{mean})^2 + (k_2 - k_{mean})^2 + (k_3 - k_{mean})^2]/3}$ and $P = k_1/k_3$, and the shape of the AMS ellipsoid by $U = (2k_2 - k_1 - k_3)/(k_1 - k_3)$ [*Jelinek,* 1981; 1984]. Even small amounts of ferromagnetic inclusions can dominate the low-field AMS. For this reason, high-field AMS was measured in addition to low-field AMS. High-field methods make it possible to isolate the component of the AMS carried by paramagnetic minerals alone. The high-field measurements were performed on a torque magnetometer, in various fields between 1.0 T and 1.5 T [*Bergmüller et al.*, 1994]. In such high fields, the ferromagnetic magnetization is saturated, while the paramagnetic magnetization increases with the applied field. The different field-dependence allows for separation of the ferromagnetic from the paramagnetic components [*Martín-Hernández and Hirt,* 2001]. High-field AMS was determined both at

197 room temperature (RT) and at 77 K and is described by *k'* and *U* like the low-field AMS. At
198 low temperature, the paramagnetic signal is enhanced [*Schmidt et al.*, 2007b]. This
199 enhancement can be quantified by $p'_{77} = \frac{k'(77K)}{k'(RT)}$.

200 # 3 Results

201 ## 3.1 Chemistry

202 Average chemical compositions are summarized in Table A (Online Supplementary).
203 Whereas some samples show zonation, most are homogeneous on a crystal scale. The only
204 exception is hypersthene (samples Hyp1 and Hyp2), which consists of Ca-rich clinopyroxene
205 exsolution lamellae and Ca-poor orthopyroxene. For these samples, the composition given in
206 Table A is the average of all measurements, hence represents the average high-temperature
207 composition prior to exsolution. One augite, NMB46281, was too large to fit the ablation
208 chamber and could thus not be analyzed by LA-ICP-MS. The samples cover a wide range of
209 Fe concentrations, which lie between 0.005 and 29.6 wt.% FeO in the clinopyroxene and
210 between 0.6 and 15.3 wt.% FeO in the orthopyroxene group. Other elements with strong
211 magnetic moments were only present in small amounts: MnO < 0.7 and 0.3 wt.%, Cr < 4050
212 and < 3000 µg/g and Ni < 2020 and < 1450 µg/g in clino- and orthopyroxene, respectively.

213 Representative Mössbauer spectra and fits are shown in Figure 2, and hyperfine
214 parameters are given in Table 2. The spectra exhibit different characteristics for diopside,
215 augite and aegirine. The diopside samples exhibit one dominant doublet (one high spin Fe^{2+})
216 and one unresolved Fe^{3+} doublet overlapping the low velocity line of the Fe^{2+} doublet, which
217 yields 66 % Fe^{2+} and 34 % Fe^{3+} in the two samples. The augite samples exhibit three
218 absorption peaks that are interpreted to be an overlap of two doublet components (one high

219 spin Fe^{2+} and one high spin Fe^{3+}) resulting in Fe^{2+} areas between ca. 60 and 80 % and Fe^{3+}
220 areas between ca. 40 and 20 %. The aegerine samples exhibit one dominant doublet of high
221 spin Fe^{3+}, one minor, partially resolved Fe^{2+}, and one minor, unresolved Fe^{2+} resulting in 80
222 to 87 % Fe^{3+} and 13 to 21% Fe^{2+} in two sites. Different interpretations have been proposed for
223 the varying doublets in clinopyroxenes [e.g. *Abdu and Hawthorne*, 2013; *Redhammer et al.*,
224 2006], but because the main interest in this study lies on the relative proportions of Fe^{2+} and
225 Fe^{3+}, they will not be discussed further.

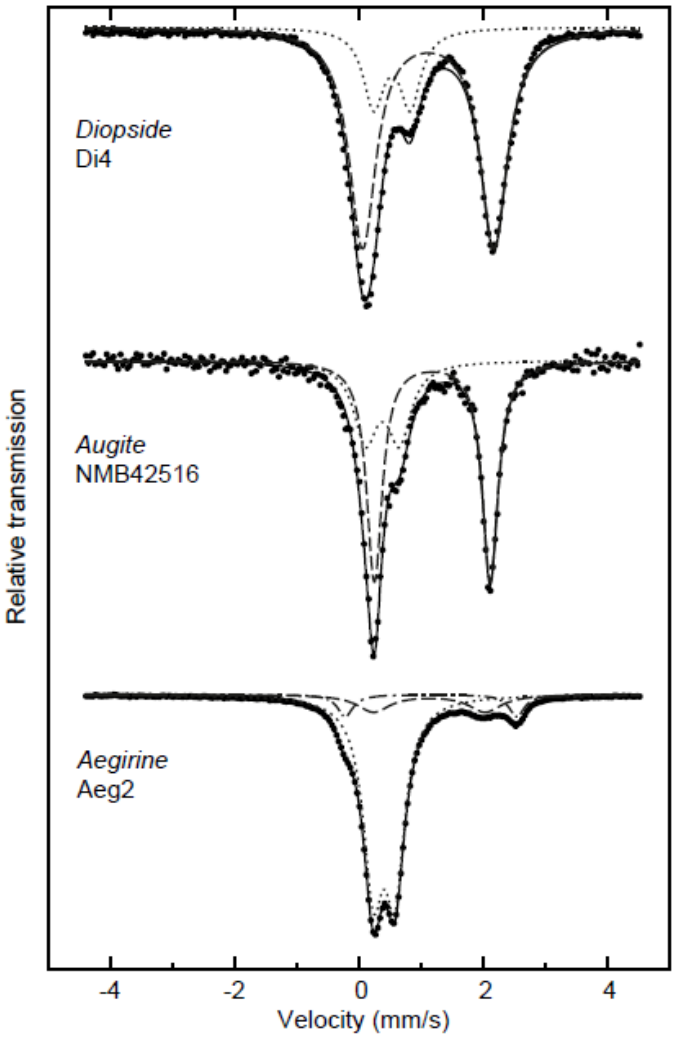

226

227 *Figure 2: Characteristic Mössbauer spectra for selected samples.*
228

229 Recalculated site occupancies are shown in Table B (Online Supplementary). The M2
230 sites of diopside and augite are mainly filled with Ca; however, not all samples contain
231 enough Ca to occupy all M2 sites. Fe^{2+} preferentially fills this Ca-vacancy, but in general the
232 Fe^{2+} concentration is higher in M1 than in M2 [*Burns*, 1993]. Therefore, and in accordance
233 with *Deer et al.* [1978], all Fe^{2+} is assigned to the M1 sites. The dominant cation in the M1
234 sites is Mg for diopside, and various combinations of Mg, Al and Fe^{2+} in the augite samples.
235 In aegirine, Na replaces Ca in the M2 sites, and the M1 sites contain mainly Fe. In the ideal
236 formula, the latter is present as Fe^{3+}, which is confirmed by Mössbauer data on selected
237 crystals. The M1 sites in spodumene are filled mainly by Al and the M2 sites by Li. For
238 enstatite, only very small amounts of Ca are present and both M1 and M2 sites are occupied
239 by Mg or Fe. In this configuration, Fe^{2+} prefers M2 sites, whereas Fe^{3+} and Al are
240 preferentially located in M1 [*Deer et al.*, 1978]. The site occupancies shown for hypersthene
241 correspond to the homogeneous high-temperature orthopyroxene prior to exsolution.

242 **3.2 Mass susceptibility**

243 Mean mass susceptibility in clinopyroxene ranges from $-5.86*10^{-9}$ m^3/kg to $6.98*10^{-6}$
244 m^3/kg for diopside, $-3.78*10^{-8}$ m^3/kg - $1.00*10^{-8}$ m^3/kg for spodumene, $5.68*10^{-7}$ m^3/kg –
245 $6.73*10^{-7}$ m^3/kg for aegirine, and covers a wide range from $1.57*10^{-7}$ m^3/kg to $2.73*10^{-5}$
246 m^3/kg in augite. One diopside and six spodumene crystals are diamagnetic. For
247 orthopyroxene, the mean susceptibility lies between $7.00*10^{-9}$ m^3/kg and $1.08*10^{-6}$ m^3/kg
248 (Table 3). According to *Vernon* [1961] and *Bleil and Petersen* [1982], the susceptibility of a
249 paramagnetic material can be calculated based on the concentration of strongly magnetic ions
250 such as Fe or Mn. In the crystal collection in this study, the concentrations of Mn or other
251 cations with strong magnetic moments are low (Table A); thus the paramagnetic susceptibility
252 can be estimated based on Fe concentration alone. For clinopyroxene, the effective magnetic
253 moment of Fe^{2+} is $6.06\mu_B$ and for orthopyroxene it is $5.08\mu_B$ [*Parks and Akhtar*, 1968]. No

experimental values are available for the effective magnetic moment of Fe^{3+} in pyroxenes and therefore the theoretical value of $5.88\mu_B$ is used [*Parks and Akhtar*, 1968; *Vernon*, 1961]. Thus, the theoretical paramagnetic susceptibility can be computed as $\chi = 2.70*10^{-8}$*Fe m^3/kg for diopside, augite and spodumene, $2.54*10^{-8}$*Fe m^3/kg for aegirine and $1.89*10^{-8}$*Fe m^3/kg for orthopyroxene, where Fe is the Fe concentration in weight percent. A good agreement between calculated and measured susceptibilities was found for diopside and enstatite (Table 3, Figure 3). The calculation does not take into account the diamagnetic component, and therefore the theoretical susceptibility for spodumene is larger than that measured. For aegirine, the calculated susceptibility is generally lower than the measured one. This might be related to the fact that the effective magnetic moment is not well defined for Fe^{3+} in clinopyroxene in general, and specifically in aegirine. All augite crystals and one diopside have significantly larger susceptibilities than expected; these can be attributed to ferromagnetic inclusions in the crystals (Figure 3a, inset).

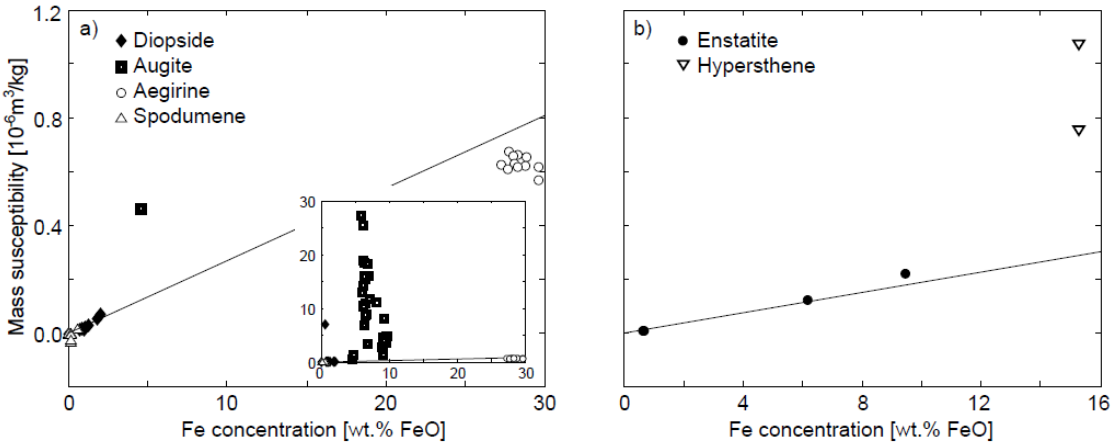

Figure 3: Mean mass susceptibility as a function of Fe concentration for a) clinopyroxene, where the inset shows the large variation in susceptibility for some samples, particularly augite; and b) orthopyroxene. Solid lines represent theoretical susceptibility based on Fe concentration and assuming that Fe is present as Fe^{2+}.

3.3 Identification of ferromagnetic inclusions

IRM increases rapidly in low fields and remanent coercivity is low for all crystals except Aeg3, whose remanent coercivity is 185 mT. The augite and hypersthene samples show the highest IRM and exhibit remanent coercivities < 20 mT. This is indicative of a low coercivity phase, typically magnetite or maghemite. The ferromagnetic inclusions in Di5, Spod1, Aeg6 and En1 have higher remanent coercivities between 30 and 40 mT, which are still in the range expected for magnetite and maghemite. Their IRM is about four orders of magnitude lower than that of the augite and hypersthene samples. Saturation is reached below 1.0 T for most samples. However, the magnetization of En1 is approaching magnetic saturation up to 2.0 T, and Aeg3 is dominated by a high coercivity phase that is only approaching saturation above 1.4 T (Figure 4). In the samples with high IRM, the main remanence carrier reaches saturation below 1.0 T, which is a prerequisite for separation of ferromagnetic and paramagnetic contributions to the magnetic anisotropy.

3.4 Low-field AMS

Principal directions of the low-field AMS are shown in Figure 5 for each mineral group. The low-field principal directions are consistent for diopside; k_2 is parallel to the crystallographic *b*–axis, and k_1 and k_3 cluster at ca. ±45° from the *c*-axis within the *a*-*c*-plane. Augite shows a large variability in low-field principal directions. Part of the samples show a grouping of minimum susceptibility parallel to the crystallographic *b*-axis. In aegirine, the maximum low-field susceptibility clusters close to the *c*-axis, and the minimum is close to the crystallographic *a**-axis. Principal directions in spodumene are variable. The maximum principal axis of enstatite groups around the crystallographic *c*-axis. AMS shapes cover the whole range from prolate to oblate, especially for samples with weak anisotropy (Figure 6).

296 Many augites have oblate AMS ellipsoids, whereas those of the orthopyroxenes are prolate

297 (Table 3).

298

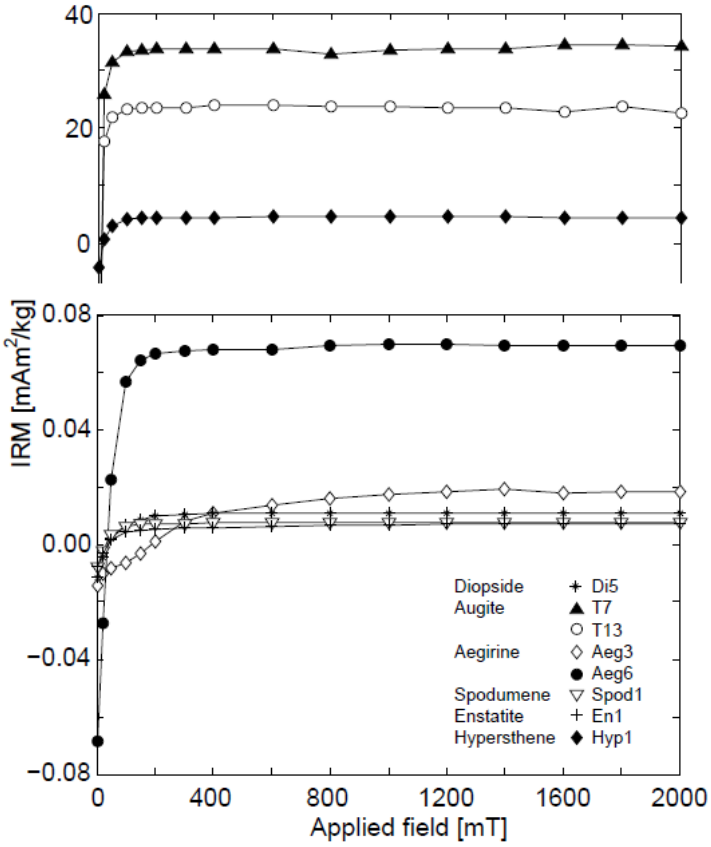

299

300 *Figure 4: Isothermal remanent magnetization (IRM) acquisition curves for representative clino- and*
301 *orthopyroxene samples.*

302

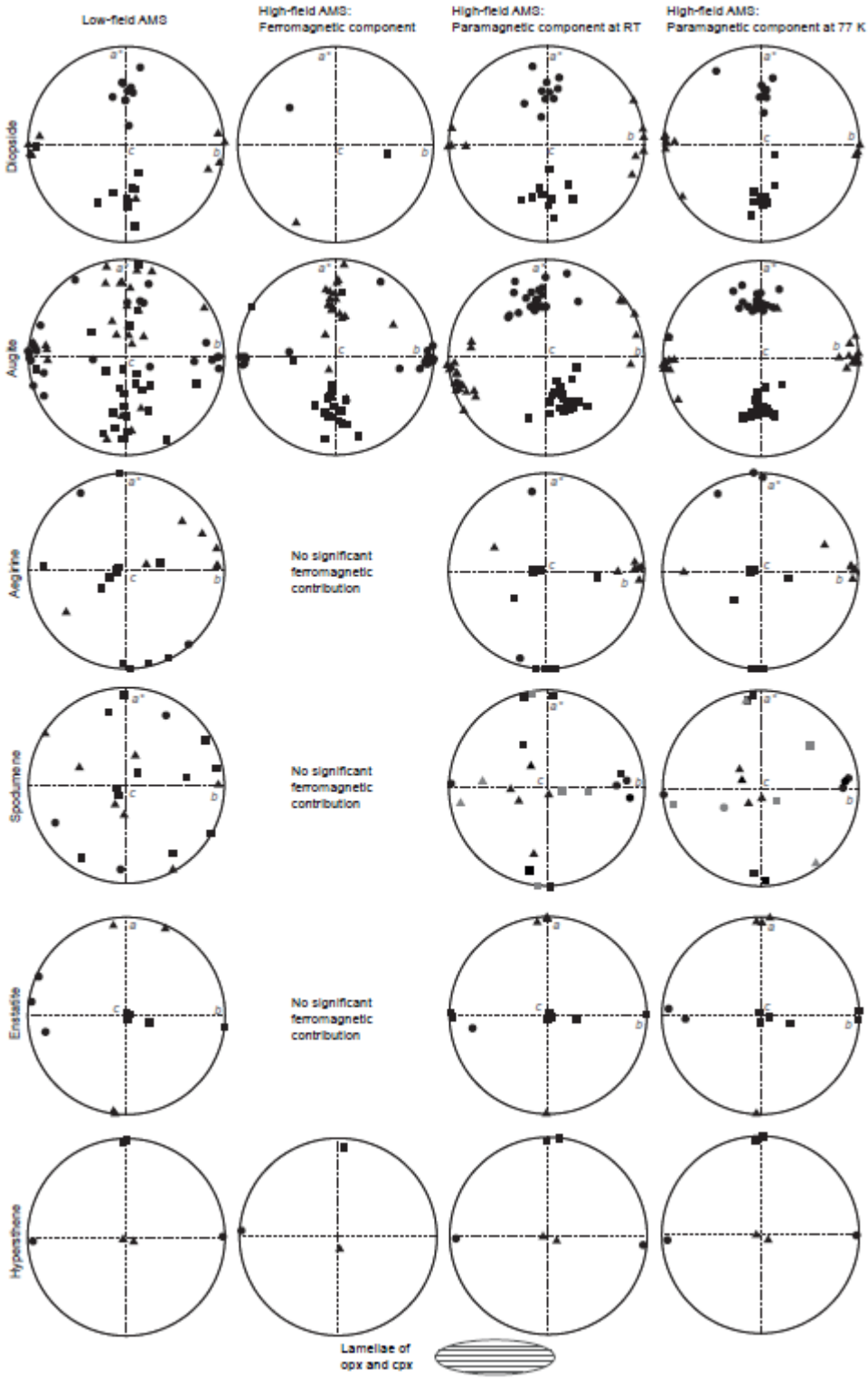

303

304 *Figure 5: Equal area lower hemisphere stereoplots showing principal susceptibility directions for low-*
305 *field AMS, ferromagnetic component of the high-field AMS at RT and paramagnetic component of the*
306 *high-field AMS at RT and 77 K for each mineral group. Directions are given in a crystallographic*
307 *reference frame or relative to the orientation of the lamellae in hypersthene.*
308

3.5 Ferrimagnetic AMS

One sample each of diopside and hypersthene, and most augite crystals exhibit a significant ferromagnetic contribution to the high-field AMS. This ferromagnetic component was isolated and directions of the ferromagnetic principal susceptibilities are plotted in Figure 5. In most crystals, the minimum susceptibility of the ferromagnetic component is parallel to the crystallographic *b*-axis of the clinopyroxene. The maximum and intermediate ferromagnetic susceptibilities lie in the *a*-*c* plane, at a ca. 45° angle to the crystallographic *c*-axis. In hypersthene, the minimum and intermediate ferromagnetic susceptibilities lie in the plane of the exsolution lamellae, and the maximum normal to this plane. With two exceptions, the shape of the ferromagnetic AMS is oblate. The ferromagnetic anisotropy degree *k'* varies from $3.01*10^{-10}$ m^3/kg to $5.04*10^{-8} m^3/kg$ (Table 4).

3.6 Paramagnetic AMS

The paramagnetic component of the AMS was separated from the high-field AMS both at room temperature and at 77 K. Principal paramagnetic directions for each mineral group are shown in Figure 5, and the shape of the AMS ellipsoid and degree of anisotropy are show in Figure 6. Table 5 summarizes principal directions and AMS degree and shape parameters.

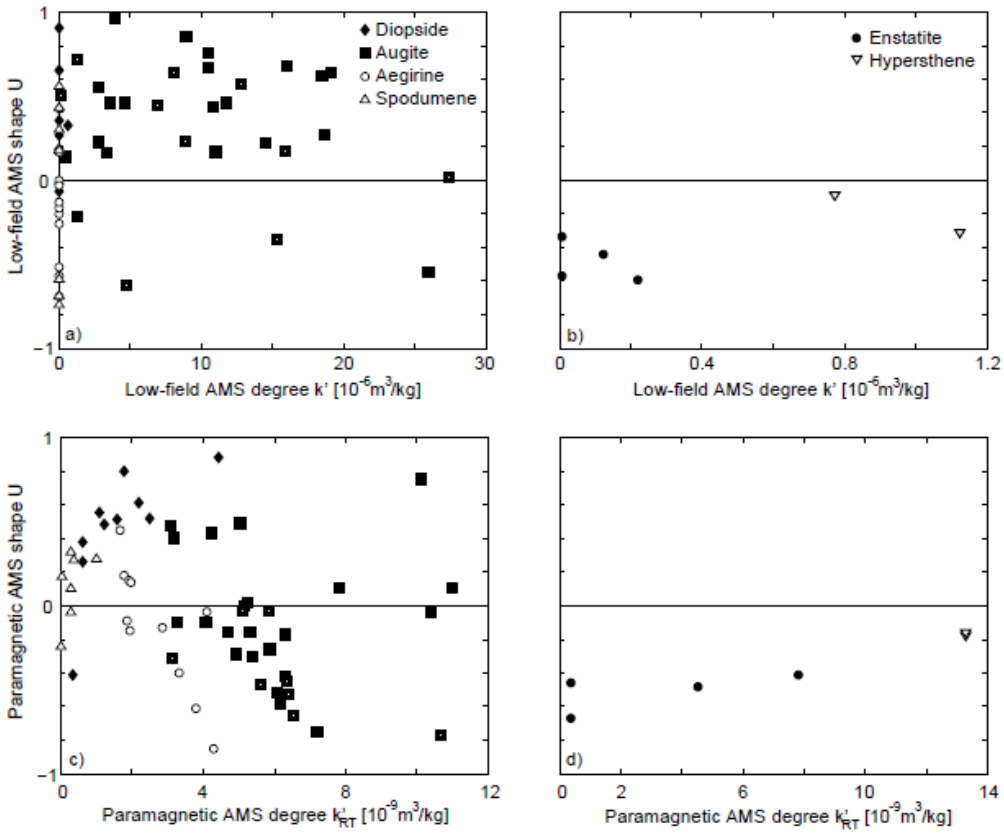

Figure 6: Modified Jelinek plot for low-field AMS (a,b) and isolated paramagnetic AMS at RT (c,d). Data is plotted for clinopyroxene (a,c) and orthopyroxene (b,d).

3.6.1 Clinopyroxene

For diopside and augite, the intermediate principal susceptibility is generally parallel to the crystallographic *b*-axis, and k_1 and k_3 lie in the *a*-*c*-plane, with k_1 approximately 45° inclined towards the –*a**-axis with respect to the *c*-axis. The directions are better grouped at 77 K, where the paramagnetic signal is enhanced. Interestingly, the principal directions are rotated ca. 20° anticlockwise with respect to the principal directions for augite at room temperature. Diopside AMS is oblate for all samples except Di2, which is diamagnetic. Augite generally displays a prolate AMS ellipsoid. The degree of deviatoric susceptibility *k'* varies from $3.48*10^{-10}$ m^3/kg to $4.45*10^{-9}$ m^3/kg at room temperature in diopside and increases by a factor of 2.71 upon cooling to 77 K for Di2 and between 10.8 and 14.4 for the

other diopside crystals. In augite, k' is larger and ranges from $3.09*10^{-9}$ m^3/kg to $1.10*10^{-8}$ m^3/kg at room temperature. The increase in k' when cooling to 77 K as defined by p_{77}' is between 5.3 and 20.4, with the majority of samples showing p_{77}' between 11 and 17.

The principal susceptibility axes are oriented differently in aegirine: k_1 is parallel to the crystallographic *c*-axis, k_2 parallel to the *b*-axis and k_3 parallel to the *a**-axis. The directions group well for the larger crystals (> 4 g), whereas those of the smaller samples (< 0.5 g) are more scattered. AMS shapes cover a wide range from prolate to oblate, and k' varies from $1.67*10^{-9}$ m^3/kg to $4.29*10^{-9}$ m^3/kg. The deviatoric susceptibility is 8.30 – 11.65 times larger at 77 K.

Two types of behavior can be seen in spodumene; the Fe-richer varieties have the minimum susceptibility parallel to the *b*-axis, whereas the Fe-poor ones have k_3 parallel to *a** at RT, but close to *c* at 77 K. AMS shapes vary considerably for individual samples, which is attributed to their weak susceptibility. The anisotropy degree k' ranges from $2.66*10^{-11}$ m^3/kg to $1.01*10^{-9}$ m^3/kg at room temperature and increases 5.54 to 20.75 times when measured at 77 K. The large increase in Spod1 and Spod2 relates to the contribution of a diamagnetic component at RT.

The degree of the paramagnetic AMS k' shows a general increase with Fe concentration for spodumene, diopside and augite (Figure 7). Therefore, k' can be estimated from the Fe concentration by

$$k' = 8.28*10^{-10}*Fe \ m^3/kg$$

where *Fe* is the Fe concentration in wt.% FeO. Aegirine possesses a lower degree of anisotropy than predicted by this trend, which is discussed below.

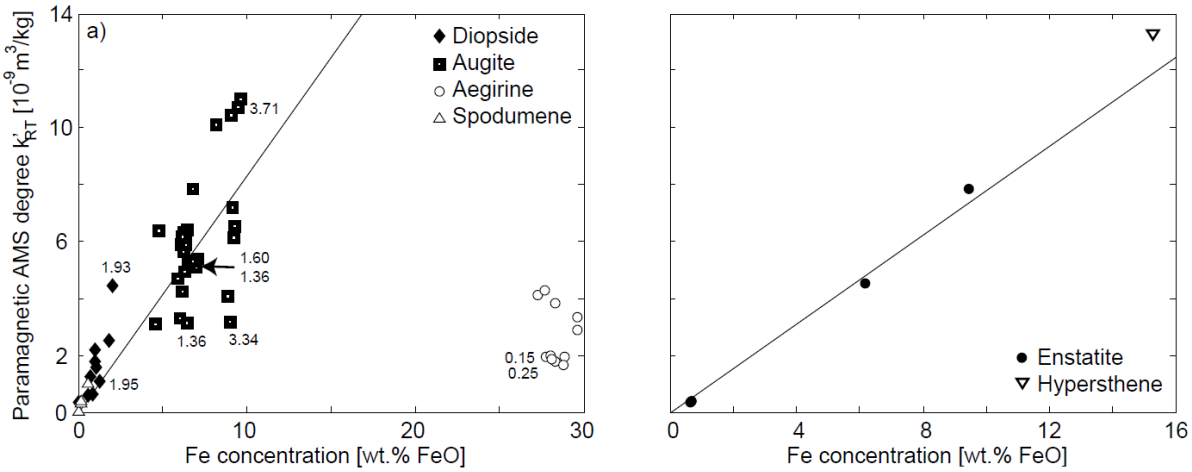

Figure 7: Anisotropy degree (k') as a function of Fe concentration for a) clinopyroxene, in which Fe^{2+}/Fe^{3+} ratios are shown where available; and b) orthopyroxene.

3.6.2 Orthopyroxene

Enstatite has its maximum principal susceptibility parallel to *c*, the intermediate susceptibility parallel to the *a*-axis and minimum parallel to the *b*-axis, both at room temperature and at 77 K. The AMS ellipsoid has a prolate shape and *k'* varies between $3.67*10^{-10}$ m^3/kg and $7.83*10^{-9}$ m^3/kg. The anisotropy increases by a factor of 7.27 – 8.63 when the measurement temperature is 77 K compared to room temperature.

The maximum susceptibility of hypersthene, which consists of lamellae of orthopyroxene and Ca-rich clinopyroxene, is normal to these exsolution lamellae, whereas k_2 and k_3 lie in the plane of the lamellae. For hypersthene, the AMS has a less prolate shape than for enstatite, probably due to a superposition of the orthopyroxene and clinopyroxene anisotropies. p_{77}' varies between 7.27 and 7.31.

Similar to the clinopyroxene crystals, *k'* of enstatite increases with Fe concentration (Figure 7b):

$k' = 7.80*10^{-10}*Fe$ m^3/kg.

382 Hypersthene has a slightly higher AMS degree than expected from the enstatite trend and its
383 Fe concentration. This may be explained by the superposition of clino- and orthopyroxene
384 anisotropy, as *k'* is larger for clinopyroxene than orthopyroxene for a given Fe content.

385 # 4 Discussion

386 ## 4.1 Mass susceptibility and chemical composition

387 *Vernon* [1961] proposed that magnetic susceptibility can be used as a measure of Fe
388 and Mn contents in silicates. A good correlation is observed between Fe concentration and
389 susceptibility in diopside, aegirine and enstatite. In augite and hypersthene, however, the
390 susceptibility appears to be mainly controlled by the amount of ferromagnetic inclusions, such
391 as magnetite, within the crystals. This effect is larger than the dependence on Fe concentration
392 in the structure and illustrates the importance of knowing which mineral carries the magnetic
393 susceptibility. In the absence of ferromagnetic inclusions within clinopyroxene or
394 orthopyroxene, the mass susceptibility shows a good linear correlation with Fe concentration.

395 ## 4.2 Paramagnetic anisotropy degree and its dependence on Fe concentration

396 The degree of anisotropy, *k'*, increases with Fe concentration in both clinopyroxene,
397 with the exception of aegirine, and orthopyroxene. There is a larger variation in this
398 relationship in clinopyroxene (Figure 7), whereas it is more linear in enstatite. Aegirine has a
399 small anisotropy degree given its large Fe content. Mössbauer spectroscopy revealed that
400 aegirine mainly contains Fe^{3+}, whereas Fe^{2+} dominates in the diopside-augite series. It has
401 been argued that Fe^{2+} possesses a strong ionic magnetic anisotropy in the trigonal crystal field
402 in micas, whereas Fe^{3+} is isotropic [*Ballet and Coey*, 1982; *Beausoleil et al.*, 1983]. Because
403 the M1 sites in clinopyroxene are similar to the M2 sites in biotite in terms of the crystal field
404 to which the cation is subjected [*Burns*, 1993], a similar argument could hold for aegirine.
405 Therefore, if the Fe^{3+} in aegirine is isotropic, only Fe^{2+} would cause an anisotropy. The

presence of Fe^{3+}, hence variable Fe^{2+}/Fe^{3+}, may also explain some of the scatter in *k'* found in the diopside and augite crystals that have similar total Fe concentration. Orthopyroxene rarely incorporates Fe^{3+} and thus shows a better constrained linear relationship between AMS degree and Fe concentration.

The degree of anisotropy increases by varying amounts at 77 K, with an increase between 3 and 21 in the diopside-augite series; 8 and 12 for aegirine; and 5 and 21 for spodumene. No clear dependence is found between p_{77}' and Fe concentration in clinopyroxenes (Figure 8). The diopside Di2 and spodumene NMB444 show low p_{77}' values of 2.71 and 5.54, respectively. The spodumene crystals Spod1 and Spod2 display large p_{77}' between 12.23 and 20.75. Together with the negative or weak positive mean susceptibilities, this suggests a contribution of a temperature-independent diamagnetic AMS in these crystals. Interestingly, p_{77}' is close to 8 in all orthopyroxenes, a value that is similar to p_{77} found in siderite [*Schmidt et al.*, 2007a], the sheet silicate minerals muscovite, phlogopite and chlorite [*Biedermann et al.*, 2014a], olivine [*Biedermann et al.*, 2014b], and some members of the amphibole group [*Biedermann et al.*, in review].

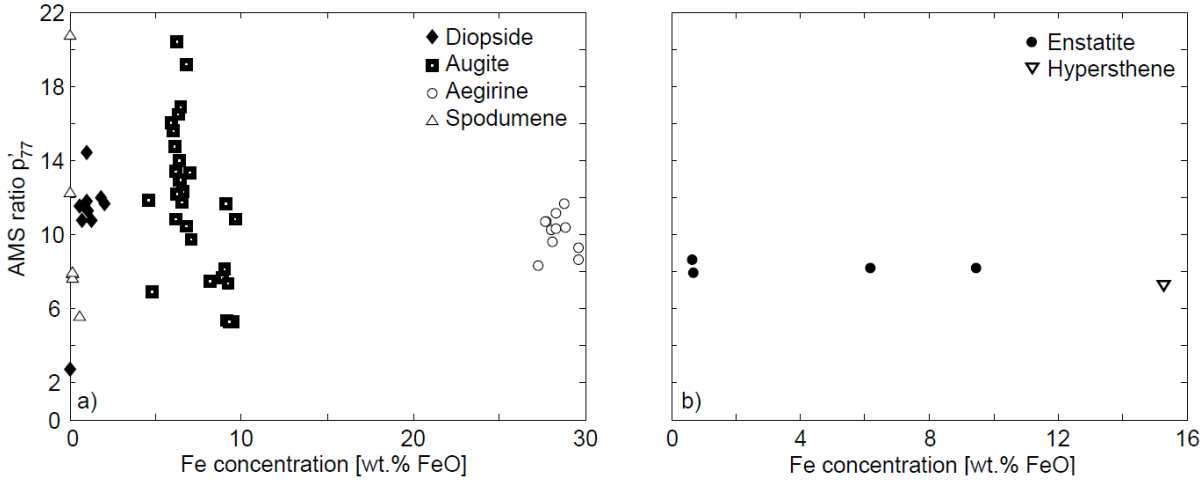

Figure 8: Factor p_{77}' as a function of Fe concentration for the different mineral groups: a) clinopyroxene and b) orthopyroxene.

425 **4.3 Paramagnetic principal directions and crystal structure**

426 In clinopyroxene, which possesses monoclinic symmetry, one of the principal
427 susceptibility directions has to be parallel to the crystallographic *b*-axis, whereas there are no
428 constraints on the other two principal susceptibility directions. These constraints are imposed
429 by crystal symmetry [*Neumann*, 1885; *Nye*, 1957]. The paramagnetic k_2-axes are parallel to
430 the *b*-axis in diopside, and the minimum and maximum susceptibilities lie in the *a*-*c*-plane.
431 The principal axes of the AMS ellipsoid of augite show a similar orientation at 77 K, but the
432 susceptibility tensor is rotated at room temperature; k_2 is rotated up to 40° away from *b*.
433 Crystal symmetry does not allow this rotation, which occurs only in those samples with
434 significant ferromagnetic contributions. Therefore we suggest that the rotation represents an
435 artefact related to the ferromagnetic inclusions, i.e. that the magnetic field is disturbed locally
436 by their strong magnetization. The principal directions determined in this study agree with the
437 orientation of the k_2-axis proposed by *Parry* [1971] and *Lagroix and Borradaile* [2000], but
438 not with the orientation of k_1 described by *Finke* [1909]. In addition, the results presented here
439 show that not only k_2, but also k_1 and k_3 have clearly defined orientations with respect to the
440 crystal lattice.

441 In aegirine, all three principal paramagnetic susceptibilities are parallel to one
442 crystallographic axis, and thus the symmetry of the susceptibility tensor is higher than
443 required by crystal symmetry. The difference in orientation of the principal axes compared to
444 the diopside-augite series may be explained by the different predominant oxidation state of
445 Fe, or by small changes in the unit cell imposed by the different sizes and charge of Ca and
446 Na cations on the M2 site.

447 Interestingly, the different orientation of the susceptibility tensor with respect to
448 crystal lattice in aegirine as opposed to the diopside-augite series is in agreement with the

orientation of the optical indicatrix in these minerals. In aegirine, the principal axes of the indicatrix are inclined 0-10° with respect to the *c* and *a** crystallographic axes and in diopside-augite the inclination varies between 35° and 48° [*Tröger*, 1982]. Even though maximum and minimum susceptibility do not always coincide with the same indicatrix axes, this confirms the crystallographic control of the magnetic anisotropy. More work would be needed, however, in order to understand why k_1 is oriented at a 45° angle from the crystallographic *c*-axis in diopside and augite.

The magnetic anisotropy in spodumene is a superposition of a diamagnetic and a paramagnetic component. Principal directions are consistent for samples with similar Fe concentrations, i.e. for Spod1 and Spod2 with 0.005 wt.% FeO, or for the group with 0.2 – 0.6 wt.% FeO consisting of Spod3-4, NMB444 and fXl and fXl2, but differ between the groups. Because Spod1 and Spod2 have the lowest Fe concentration, their anisotropy ellipsoids may represent the diamagnetic fraction of the susceptibility.

For orthopyroxene, the principal directions of any second-order tensor property are each parallel to one of the crystallographic axes, as required by the orthorhombic symmetry. Enstatite has its maximum susceptibility aligned with the crystallographic *c*-axis, and k_2 and k_3 are parallel to the *a*- and *b*-axes, respectively. One sample deviates from this general behavior, which is due to a small misorientation of the crystal. *Lagroix and Borradaile* [2000] have already proposed the alignment of k_1 parallel to *c*. However, they did not find any relation between k_2 and k_3 with the *a*- or *b*-axes, violating crystal symmetry constraints. They explained this by the effects of ferromagnetic inclusions or misorientation. Isolating the paramagnetic anisotropy demonstrates that k_3 is parallel to the crystallographic *b*-axis in enstatite. These results seemingly contradict findings by *Wiedenmann et al.* [1986], who measured Fe-rich orthopyroxenes and found that the maximum susceptibility is parallel to *b*.

Their samples differ considerably from this collection, however, because they have a significantly larger Fe concentration and both M1 and M2 sites are occupied predominantly by Fe. Crystals used in this study have small Fe concentrations and the Fe is located mainly in M2 sites.

4.4 Ferromagnetic inclusions

Many pyroxenes, especially augite, contain ferromagnetic inclusions, which, even when their abundances are small, clearly dominate the magnetic susceptibility and its anisotropy in low fields. There are two principal types of occurrence of magnetite in augite, (1) accidental magnetite inclusions (incorporated in augite during crystal growth), and (2) magnetite forming as exsolution products upon cooling of augite crystals, where the magnetite (111) plane often lies parallel to (100) of the augite, and (-110) parallel to (010). If there are needles of magnetite, these lie in the (010) plane and are elongated parallel or perpendicular to [001] [*Bown and Gay*, 1959; *Deer et al.*, 1978; *Feinberg et al.*, 2004; *Feinberg et al.*, 2006]. The consistency of ferromagnetic principal susceptibility directions exhibited by the samples thus suggests that magnetite inclusion of type (2) predominates.

If clinopyroxene is preferentially oriented in a rock, and type (2) magnetite inclusions within this pyroxene carry a remanent magnetization, the recorded paleomagnetic direction could be deflected away from the direction of the magnetizing field. Furthermore, paleointensity studies made on single pyroxene crystals may yield inconsistent results when an isotropic susceptibility is assumed. Thus, paleomagnetic studies in rocks with a strong mineral fabric need to consider this aspect when interpreting paleomagnetic data.

5 Conclusions

The paramagnetic anisotropy in clinopyroxenes and orthopyroxenes is clearly related to the crystal lattice of each mineral group and to the concentration, dominant site distribution

and oxidation state of Fe in each mineral. In clinopyroxene, the Fe atoms are located mainly in M1 sites and the directions of the principal susceptibilities are k_2 // b and k_1, k_3 in the a-c-plane in the diopside-augite series and k_1 // c, k_2 // b and k_3 // a^* in aegirine. There is a general trend of increasing AMS degree with increasing Fe concentration. The AMS degree is, however, affected by the Fe^{2+}/Fe^{3+} ratio, which results in a low AMS degree for aegirine, due to its large Fe^{3+} concentration. In enstatite, the maximum susceptibility is parallel to the crystallographic c-axis, and the intermediate and minimum susceptibilities are aligned with a- and b-axes, respectively. The AMS degree increases nearly linearly with Fe concentration. These results can be used together with orientation distribution functions of the respective minerals in order to model paramagnetic anisotropy in a pyroxene-bearing rock. Further, they will help interpreting AMS, e.g. in ultramafic and mafic rocks in terms of crystallographic preferred orientation of the pyroxenes.

This study demonstrates that ferromagnetic inclusions are present mainly in augite, and that preferred orientation of these inclusions causes a strong ferromagnetic anisotropy. This may dominate the low-field anisotropy and mask the anisotropy originating from the paramagnetic pyroxene. Therefore, if AMS is used as a proxy for pyroxene texture, it is necessary to isolate the paramagnetic contribution to the total magnetic anisotropy. The confinement of magnetite within the pyroxene lattice also should be considered in paleomagnetic studies employing rock samples with oriented pyroxene crystals.

Acknowledgments

A. Puschnig (Natural History Museum Basel), A. Stucki (Siber+Siber Aathal), P. Brack and S. Bosshard (ETH Zurich) kindly provided samples for this study. We are grateful to D. Logvinovich (Laboratory of Crystallography, ETH Zurich) for an introduction to Laue orientation and assistance during measurements. This project was funded by the Swiss National Science Foundation, project 200020_143438.

References

Abdu, Y. A., and F. C. Hawthorne (2013), Local structure in *C*2/*c* clinopyroxenes on the hedenbergite ($CaFeSi_2O_6$)-ferrosilite ($Fe_2Si_2O_6$) join: A new interpretation for the Mössbauer spectra of Ca-rich C2/c clinopyroxenes and implications for pyroxene exsolution, *American Mineralogist*, *98*, 1227-1234. doi: 10.2138/am.2013.4328.

Almqvist, B. S. G., M. Herwegh, V. Schmidt, T. Pettke, and A. M. Hirt (2010), Magnetic susceptibility as a tool to study deformed calcite with variable impurity content, *Geochemistry, Geophysics, Geosystems*, *11*(1), GC002900. doi: 10.1029/2009GC002900.

Archanjo, C. J., and J. L. Bouchez (1997), Magnetic fabrics and microstructures of the post-collisional aegirine-augite syenite Triunfo pluton, northeast Brazil, *Journal of Structural Geology*, *19*(6), 849-860. doi: 10.1016/S0191-8141(97)00008-4.

Ballet, O., and J. M. D. Coey (1982), Magnetic properties of sheet silicates; 2:1 layer minerals, *Physics and Chemistry of Minerals*, *8*, 218-229. doi: 10.1007/BF00309481.

Beausoleil, N., P. Lavallee, A. Yelon, O. Ballet, and J. M. D. Coey (1983), Magnetic properties of biotite micas, *Journal of Applied Physics*, *54*(2), 906-915. doi: 10.1063/1.332053.

Bergmüller, F., C. Bärlocher, B. Geyer, M. Grieder, F. Heller, and P. Zweifel (1994), A torque magnetometer for measurements of the high-field anisotropy of rocks and crystals, *Measurement Science and Technology*, *5*(12), 1466-1470. doi: 10.1088/0957-0233/5/12/007.

Biedermann, A. R., W. Lowrie, and A. M. Hirt (2013), A method for improving the measurement of low-field magnetic susceptibility anisotropy in weak samples, *Journal of Applied Geophysics*, *88*, 122-130. doi: 10.1016/j.jappgeo.2012.10.008.

Biedermann, A. R., C. Bender Koch, W. E. A. Lorenz, and A. M. Hirt (2014a), Low-temperature magnetic anisotropy in micas and chlorite, *Tectonophysics 629*, 63-74. doi: 10.1016/j.tecto.2014.01.015.

Biedermann, A. R., T. Pettke, E. Reusser, and A. M. Hirt (2014b), Anisotropy of magnetic susceptibility in natural olivine single crystals, *Geochemistry, Geophysics, Geosystems*. doi: 10.1002/2014GC005386.

Bleil, U., and N. Petersen (1982), Magnetische Eigenschaften der Minerale, in *Landolt-Börnstein - Numerical Data and Functional Relationships in Science and Technology - Group V: Geophysics and Space Research*, edited by G. Angenheister, Springer, Berlin - Heidelberg - New York.

Borradaile, G. J., and B. Henry (1997), Tectonic applications of magnetic susceptibility and its anisotropy, *Earth-Science Reviews*, *42*, 49-93. doi: 10.1016/S0012-8252(96)00044-X.

Bown, M. G., and P. Gay (1959), The identification of oriented inclusions in pyroxene crystals, *The American Mineralogist*, *44*, 592-602.

Burns, R. G. (1993), *Mineralogical applications of crystal field theory*, 2nd ed., Cambridge University Press, Cambridge, UK.

Deer, W. A., R. A. Howie, and J. Zussman (1978), *Single-chain silicates*, 668 pp., Longman Group Ltd, London, UK.

Feinberg, J. M., H.-R. Wenk, P. R. Renne, and G. R. Scott (2004), Epitaxial relationships of clinopyroxene-hosted magnetite determined using electron backscatter diffraction (EBSD) technique, *American Mineralogist*, *89*, 462-466.

Feinberg, J. M., R. J. Harrison, T. Kasama, R. E. Dunin-Borkowski, G. R. Scott, and P. R. Renne (2006), Effects of internal mineral structures on the magnetic remanence of

571 silicate-hosted titanomagnetite inclusions: An electron holography study, *Journal of*
572 *Geophysical Research*, *111*(B12). doi: 10.1029/2006JB004498.
573 Finke, W. (1909), Magnetische Messungen an Platinmetallen und monoklinen Kristallen,
574 insbesondere der Eisen-, Kobalt- und Nickelsalze, *Annalen der Physik*, *336*(1), 149-
575 168. doi: 10.1002/andp.19093360108.
576 Guillong, M., D. L. Meier, M. M. Allan, C. A. Heinrich, and B. W. D. Yardley (2008),
577 SILLS: A MATLAB-based program for the reduction of laser ablation ICP-MS data of
578 homogeneous materials and inclusions, *Miner. Assoc. Canada Short Course*, *40*, 328-
579 333.
580 Hrouda, F. (1982), Magnetic anisotropy of rocks and its application in geology and
581 geophysics, *Geophysical Surveys*, *5*, 37-82. doi: 10.1007/BF01450244.
582 Jelinek, V. (1981), Characterization of the magnetic fabric of rocks, *Tectonophysics*, *79*, T63-
583 T67. doi: 10.1016/0040-1951(81)90110-4.
584 Jelinek, V. (1984), On a mixed quadratic invariant of the magnetic susceptibility tensor,
585 *Journal of Geophysics - Zeitschrift Fur Geophysik*, *56*(1), 58-60.
586 Lagroix, F., and G. J. Borradaile (2000), Magnetic fabric interpretation complicated by
587 inclusions in mafic silicates, *Tectonophysics*, *325*, 207-225. doi: 10.1016/S0040-
588 1951(00)00125-6.
589 Laugier, J., and A. Filhol (1983), An interactive program for the interpretation and simulation
590 of Laue patterns, *Journal of Applied Crystallography*, *16*, 281-283. doi:
591 10.1107/S0021889883010420.
592 Martín-Hernández, F., and A. M. Hirt (2001), Separation of ferrimagnetic and paramagnetic
593 anisotropies using a high-field torsion magnetometer, *Tectonophysics*, *337*(3-4), 209-
594 221. doi: 10.1016/S0040-1951(01)00116-0.
595 Neumann, F. E. (Ed.) (1885), *Vorlesungen über die Theorie der Elastizität der festen Körper*
596 *und des Lichtäthers*, B.G. Teubner Verlag, Leipzig, Germany.
597 Nye, J. F. (1957), *Physical properties of crystals: Their representation by tensors and*
598 *matrices*, 322 pp., Clarendon Press, Oxford, UK.
599 Parks, G. A., and S. Akhtar (1968), Magnetic moment of Fe^{2+} in paramagnetic minerals, *The*
600 *American Mineralogist*, *53*, 406-415.
601 Parry, G. R. (1971), The magnetic anisotropy of some deformed rocks, unpublished PhD
602 thesis thesis, 218 pp, University of Birmingham, Birmingham, UK.
603 Pettke, T., F. Oberli, A. Audetat, M. Guillong, A. Simon, J. Hanley, and L. M. Klemm (2012),
604 Recent developments in element concentration and isotope ratio analysis of individual
605 fluid inclusions by laser ablation single and multiple collector ICP–MS, *Ore Geol.*
606 *Rev.*, *44*, 10-38. doi: 10.1016/j.oregeorev.2011.11.001.
607 Redhammer, G. J., G. Amthauer, G. Roth, G. Tippelt, and W. Lottermoser (2006), Single-
608 crystal X-ray diffraction and temperature dependent ^{57}Fe Mössbauer spectroscopy on
609 the hedenbergite-aegirine $(Ca,Na)(Fe^{2+},Fe^{3+})Si_2O_6$ solid solution, *American*
610 *Mineralogist*, *91*, 1271-1292. doi: 10.2138/am.2006.2173.
611 Schmidt, V., A. M. Hirt, K. Hametner, and D. Gunther (2007a), Magnetic anisotropy of
612 carbonate minerals at room temperature and 77 K, *American Mineralogist*, *92*(10),
613 1673-1684. doi: 10.2138/am.2007.2569.
614 Schmidt, V., A. M. Hirt, P. Rosselli, and F. Martín-Hernández (2007b), Separation of
615 diamagnetic and paramagnetic anisotropy by high-field, low-temperature torque
616 measurements, *Geophysical Journal International*, *168*(1), 40-47. doi: 10.1111/j.1365-
617 246X.2006.03202.x.

618 Spandler, C., T. Pettke, and D. Rubatto (2011), Internal and external fluid sources for
619 eclogite-facies veins in the Monviso Meta-ophiolite, Western Alps: Implications for
620 fluid flow in subduction zones., *Journal of Petrology*, *52*, 1207-1236.
621 Tröger, W. E. (1982), *Optische Bestimmung der gesteinsbildenden Minerale. Teil 1*
622 *Bestimmungstabellen*, 5. Auflage ed., E. Schweizerbart'sche Verlagsbuchhandlung,
623 Stuttgart, Germany.
624 Vernon, R. H. (1961), Magnetic susceptibility as a measure of total iron plus manganese in
625 some ferromagnesian silicate minerals, *The American Mineralogist*, *46*, 1141-1153.
626 Wagner, J.-J., I. G. Hedley, D. Steen, C. Tinkler, and M. Vuagnat (1981), Magnetic
627 anisotropy and fabric of some progressively deformed ophiolitic gabbros, *Journal of*
628 *Geophysical Research*, *86*(B1), 307-315. doi: 10.1029/JB086iB01p00307.
629 Wiedenmann, A., J.-R. Regnard, G. Fillion, and S. S. Hafner (1986), Magnetic properties and
630 magnetic ordering of the orthopyroxenes $Fe_xMg_{1-x}SiO_3$, *Journal of Physics C: Solid*
631 *State Physics*, *19*(19), 3683-3695. doi: 10.1088/0022-3719/19/19/022.

632

633